Biochemistry and Biophysics Reports 28 (2021) 101171

Contents lists available at ScienceDirect

Biochemistry and Biophysics Reports

journal homepage: www.elsevier.com/locate/bbrep

The citrus plant pathogen *Xanthomonas citri* has a dual polyamine-binding protein

Aline Sampaio Cremonesi [a,b], Lilia I. De la Torre [b,c,d], Maximillia Frazão de Souza [e], Gabriel S. Vignoli Muniz [f], M. Teresa Lamy [f], Cristiano Luis Pinto Oliveira [e], Andrea Balan [b,*]

[a] Programa de Pós-graduação Interunidades em Biotecnologia, Universidade de São Paulo, 05508-900, SP, Brazil
[b] Laboratório de Biologia Estrutural Aplicada LBEA, Departamento de Microbiologia, Instituto de Ciências Biomédicas, Universidade de São Paulo, 05508-900, SP, Brazil
[c] Programa de Pós-graduação em Genética e Biología Molecular, Universidade Estadual de Campinas, 13083 – 970, SP, Brazil
[d] Grupo Investigaciones Biomédicas, Departamento de Biología y Química, Universidad de Sucre, 700003, Sucre, Colombia
[e] Grupo de Fluidos Complexos, Departamento de Física Experimental, Instituto de Física, Universidade de São Paulo, 05508-090, SP, Brazil
[f] Laborátorio de Biomembranas, Instituto de Física, Universidade de São Paulo, 05508-090, SP, Brazil

ARTICLE INFO

Keywords:
Polyamine binding
Substrate-binding protein
PotF
Xanthomonas citri
Spermidine
Putrescine
Ligand-induced conformational changes

ABSTRACT

ATP-Binding Cassette transporters (ABC transporters) are protein complexes involved in the import and export of different molecules, including ions, sugars, peptides, drugs, and others. Due to the diversity of substrates, they have large relevance in physiological processes such as virulence, pathogenesis, and antimicrobial resistance. In *Xanthomonas citri* subsp. *citri,* the phytopathogen responsible for the citrus canker disease, 20% of ABC transporters components are expressed under infection conditions, including the putative putrescine/polyamine ABC transporter, PotFGHI. Polyamines are ubiquitous molecules that mediate cell growth and proliferation and play important role in bacterial infections. In this work, we characterized the *X. citri* periplasmic-binding protein PotF (XAC2476) using bioinformatics, biophysical and structural methods. PotF is highly conserved in *Xanthomonas* sp. genus, and we showed it is part of a set of proteins related to the import and assimilation of polyamines in *X. citri*. The interaction of PotF with putrescine and spermidine was direct and indirectly shown through fluorescence spectroscopy analyses, and experiments of circular dichroism (CD) and small-angle X-ray scattering (SAXS), respectively. The protein showed higher affinity for spermidine than putrescine, but both ligands induced structural changes that coincided with the closing of the domains and increasing of thermal stability.

1. Introduction

Xanthomonas citri (*X. citri*) is a gram-negative phytopathogenic bacterium responsible for the citrus canker, a disease that causes significant losses of citrus fruits affecting the economy in Brazil and the World [1]. Production of xanthan gum polysaccharide [2,3] induction of adhesins [4,5] and type III and IV effector proteins are some of the many mechanisms involved in the infection and pathogenesis [6,7]. The relationship between ATP-Binding Cassette systems (ABC transporters) and physiological processes has been largely demonstrated in bacteria and also in *Xanthomonas* genus [8–12]. Proteomics analyses made from leaf extracts from plants infected with *X. citri* revealed that more than 20% of the ABC transporters from *X. citri* were expressed under infection and pathogenesis [13,14]. Among the highly expressed transporters, there are components of the putative putrescine/polyamine ABC system PotFGHI [15], encoded by *potFGHI* operon. Polyamines (putrescine, spermidine, and spermine) are ubiquitous in almost all prokaryotic and eukaryotic cells. In eukaryotes, they play roles in the synthesis and structure of nucleic acids and proteins, cell growth and viability, apoptosis among others [16]. In prokaryotes, they are capable to bind to nucleic acids and through these interactions, they mediate cell growth and proliferation [17–19], gene regulation, and differentiation [20], with an active role in the infection caused by different microorganisms [21–23]. Polyamine signals from mammalian hosts are responsible for the induction of the type III secretion system in *Pseudomonas aeruginosa* [24], one of the key determinants for virulence for this bacterium. In *E. coli*, three systems are related to polyamine import: the ABC transporters PotFGHI (specific for putrescine) and PotABCD (spermidine--preferential uptake system), responsible for maintenance of the levels of polyamines in presence of glucose, and the Puu (Put utilization

* Corresponding author.
E-mail address: abalan@usp.br (A. Balan).

https://doi.org/10.1016/j.bbrep.2021.101171
Received 17 August 2021; Received in revised form 6 November 2021; Accepted 8 November 2021

pathway) system, which imports putrescine for its utilization as an energy source in glucose depletion [18,25]. Structures of PotF and PotD, the periplasmic-binding proteins of the two ABC systems, are available and revealed that the binding site is characterized by four acidic residues that recognize the positively charged nitrogen and five aromatic side chains that anchor the methylene backbone by van der Waals interactions [26,27].

In the PotFGHI system of *X. citri,* PotF is the periplasmic-binding protein, but its ligand is not known. In this work, we focused on the functional and structural characterization of this protein, based on molecular modelling, biophysical assays, and small-angle X-ray scattering (SAXS). We produced the recombinant purified protein and showed that *X. citri* PotF binds both putrescine and spermidine. For putrescine, it was determined a $K_d = 5.9$ μM, whereas for spermidine a much higher association was observed, with an apparent $K_d \leq 2$ nM, revealing a preference for this ligand. SAXS and fluorescence spectroscopy showed that upon binding the protein undergoes significant structural changes. Based on the structural data from orthologs, we showed the similarities and differences identified in the ligand-binding pocket and vicinity that are responsible for the dual specificity. Together, the results presented in this work provide the basis for further functional studies and characterization of the role of PotF in the transport of polyamines in *X. citri* and other phytopathogens.

2. Materials and methods

2.1. Bioinformatics analysis

The sequences of genes and proteins from *X. citri, X. campestris, P. aeruginosa* and *E. coli* used in this study were obtained from Kyoto Encyclopedia of Genes and Genomes database (KEGG - http://www.genome.jp/kegg/). Table S1 (Supplementary Information) shows the KEGG references and functions of all genes. The alignments were performed using Clustal Omega Multiple Sequence Alignment program [28]. Three-dimensional models of *X. citri* PotF were built based on the structural coordinates of the *P. aeruginosa* SpuD in apo form (PDB ID: 3TTK) and in complex with putrescine (PDB ID: code 3TTM) and spermidine (PDB ID: 3TTN) [29] using the SWISS-MODEL.

2.2. DNA amplification and plasmid construction

A DNA fragment of 1053 bp containing the *potF* gene (XAC2476, GI 1156547) without the first 63 nucleotides corresponding to the signal peptide, was amplified by PCR from genomic DNA of *Xanthomonas citri* 306. The forward 5′ GGGCCCCCGCAACCTTTG 3′ and reverse 5′ CCATGGAACCACCGAGCAAC 3′ oligonucleotides, were used for the fragment amplification and insertion of the *Apa*I and *Nco*I restriction enzymes sites, respectively, in the start and final of the gene. The PCR product was cloned in pGEM®-T Easy (Promega) to generate the pGEM_potF, which was subsequently digested with *Apa*I and *Nco*I. The digested fragment was sub-cloned into the pET28a generating the pET28a_*potF* vector. The mature PotF expressed from this construct presented an N-terminal His_6-tagged. DNA sequencing was used for construct verification.

2.3. Expression of the recombinant putrescine-binding protein PotF

The pET28a_potF vector was used to transform *E. coli* Artic Express cells using the heat-shock method [30]. Pre-cultures of transformed cells were grown overnight at 37 °C and 200 r.p.m. in LB broth containing the appropriate antibiotics (50 μg/ml kanamycin and 20 μg/ml gentamicin). Two percent of the pre-cultures were used to inoculate 1 l of LB broth that was incubated at 37 °C until the optical density at 600 nm reached 0.5–0.6 when the recombinant protein expression was induced with 0.5 mM IPTG (Isopropyl β-D-1-thiogalactopyranoside), at 12 °C, 200 r.p.m. for 24 h. Cells were harvested by centrifugation at 4000×*g* for 10 min at 4 °C and stored at −20 °C for at least 4 h before the protein extraction procedure.

2.4. Extraction and purification of the His_6-tagged PotF protein

Pellet of the induced *E. coli* Artic Express cells were resuspended in affinity chromatography buffer A (50 mM sodium phosphate, pH 7.4, 150 mM NaCl, 5% glycerol, 0.1% Triton X-100, 1 mM PMSF, 5 mM Benzamidine and 1 mM β-mercaptoethanol) and incubated on ice with lysozyme (250 μg/ml) for 45 min. Cells were disrupted by 6 cycles of sonication (60% amplitude, 10-s pulses, and interval of 20 s between the pulses) and the lysate was centrifuged at 30,000×*g* for 60 min at 4 °C. The supernatants were submitted to immobilized metal affinity chromatography using an ÄKTA FPLC system (Amersham Biosciences) and the HiTrap Chelating HP 5 ml (GE) column loaded with 100 mM $NiSO_4$ and pre-equilibrated with buffer A. The column was washed with 20 ml buffer A and proteins were eluted with a 150 ml linear-gradient (0–100%) of buffer B (50 mM sodium phosphate buffer, pH 7.4, 150 mM NaCl, 5% glycerol, 1 mM PMSF, 5 mM Benzamidine, 1 mM β-mercaptoethanol and 500 mM imidazole). Fractions containing PotF were pooled, concentrated to 2 ml using a centrifugal filter device (Amicon MWCO 10 kDa), and loaded onto a Superdex 75 16/60 size exclusion chromatography (SEC) column. Isocratic elution was performed with SEC buffer (50 mM sodium phosphate buffer, pH 7.4, 150 mM NaCl, 5% glycerol and 1 mM DTT) at a flow rate of 0.3 ml/min.

2.5. Dynamic light scattering (DLS), circular dichroism (CD) and thermal shift assays

DLS data were collected at 18 °C using samples of recombinant PotF at 0.1 mg/ml diluted in buffer containing 50 mM sodium phosphate buffer pH 7.4, 150 mM NaCl and 5% glycerol. It was performed 300 accumulations of 10 s each. Far UV CD spectra were recorded on a Jasco-810 spectropolarimeter using a Peltier system PFD 425S for temperature control. 3 μM protein samples were prepared in 10 mM sodium phosphate buffer pH 7.4 and 15 mM NaCl. CD spectra were acquired at 20 °C using a 1 mm path length cell at 0.5 nm intervals over the wavelength range from 190 to 260 nm. Ellipticity is reported as the mean residual ellipticity [θ] (deg cm^2 $dmol^{-1}$). Spermidine and putrescine were added to 30 μM. Samples were subjected to thermal unfolding from 20 °C to 100 °C with spectra collected at 1 °C interval. The loss of secondary structure was followed by measuring the ellipticity at 222 nm using 0.5 °C intervals. Midpoint transition temperatures were calculated as the center of the Gaussian fit of the first derivative of the denaturation curves. Refolding assays were started at 100 °C and the temperature lowered to 10 °C with the concomitant acquisition of the ellipticity at 222 nm using 1.0 °C intervals. Spermidine and putrescine were added to 50 μM. Thermal shift assays of PotF were performed in presence of increasing concentrations of polyamines. Reactions were performed in a total volume of 25 μl using CFX96 Touch Real-Time PCR Detection System (BIO-RAD), using 5 μM of PotF protein and SYPRO™ Orange protein gel stain, 2.5 X final concentration (ThermoFisher Scientific). The cycle used was a melt ramp from 25 °C to 95 °C with increasing temperature steps of 0,5 °C. The T_m was determined using the CFX Manager™ Software. The ΔT_m values of experiments were averaged and plotted against the concentration of polyamine.

2.6. Fluorescence measurements

UV–visible absorption spectroscopy measurements. UV–visible absorption spectra were obtained with a UV–visible spectrophotometer (Varian Cary, Santa Clara, CA).

Steady-State fluorescence measurements. The fluorescence spectra were obtained with a fluorimeter (Varian Cary Eclipse, Santa Clara, CA). Samples were placed in a quartz cuvette with an optical pathway of 4 mm. The experiments were conducted at room temperature (22.5 °C),

with 1 ml samples of PotF (9 μM) in 50 mM Tris-HCl pH 8.0 and stock solutions of putrescine or spermidine (1 mM) in the same buffer solution added to the desired concentrations. Emission spectra were obtained using an excitation beam light at 295 nm. No inner filter correction was necessary [31], as absorbance values at the excitation light of 295 nm, were found to be smaller than 0.05. From the emission spectra, an apparent binding constant was obtained (K_b) by using the nonlinear least-squares method to fit the experimental data with the expression for the one-site binding model [32], equation (1). The K_d was calculated using equation (2).

$$F - F_0 = \frac{F_{max} - F_0}{2}\left\{\left(1 + \frac{C_L}{C_{PotF}} + \frac{1}{K_b C_{PotF}}\right) - \sqrt{\left(1 + \frac{C_L}{C_{PotF}} + \frac{1}{K_b C_{PotF}}\right)^2 - 4\frac{C_L}{C_{PotF}}}\right\} \quad (1)$$

$$K_d = \frac{1}{K_b} \quad (2)$$

where C_L and C_{PotF} are the ligand (putrescine or spermidine) and PotF molar concentrations, respectively; F_0, F, and F_{max} are the fluorescence intensities of PotF at a given wavelength in the absence of ligands, at a given ligand concentration, and at saturating concentration, respectively.

2.7. Small-angle X-ray scattering (SAXS)

SAXS analysis. The samples of apo PotF were placed at reusable quartz capillaries in a sample holder with a controlled temperature (20 °C). PotF samples at 5 mg/ml were diluted in 50 mM sodium phosphate buffer pH 7.4, and 150 mM NaCl. SAXS data of PotF samples containing 130 μM protein diluted in 50 mM Tris HCl buffer pH 8.0, 100 mM NaCl and 3 mM DTT (Dithiothreitol) were collected at the Beamline SAXS1 at the Synchrotron Light National Laboratory (LNLS, Campinas, SP, Brazil). Ligands were equally added at a final concentration of 300 μM. SAXS images were recorded in a 2D photon-counting detector PILATUS for individual sample exposure time of 10 s. A total of 10 images was collected for each sample and respectively for each sample buffer. The integration of the data was performed using Fit2D [33], resulting in a range of $0.013 < q < 0.47$. The data were treated using SUPERSAXS package (Oliveira, C.L.P and Pedersen, J.S; (available at http://stoa.usp.br/crislpo/files/). The final intensity data, as a function of the modulus of the reciprocal space momentum transfer q, described by $4\pi\, sin\theta/\lambda$ (where θ is the scattering angle and λ is the radiation wavelength), were analyzed with GNOM program (37) applying Indirect Fourier Transformation (IFT) for a monodisperse system.

Data analysis. The pair distribution function p(r) was computed by GNOM program [34]. The best fitting of the experimental SAXS profile was obtained assuming a monodisperse system, with maximum diameter (D_{max}) and the radius of gyration (Rg).

Fitting of SAXS data and the PotF three-dimensional structure model. The theoretical scattering curve of the modelled structure was calculated and compared with the experimental SAXS curve using the program CRYSOL [35] with entry of the crystallographic model of *P. aeruginosa* PotD (PDB 3TTM). The modelled structure was optimized against the SAXS data using the CORAL program [36]. *Ab initio* models of *X. citri* PotF were built using DAMMIN program [37], where simulated annealing method is applied to optimized dummy atom arrangement drive-by D_{max} from p(r) function and χ^2 criteria. When necessary, the alignment of the *ab initio* models was performed using SUPCOMB [38] and DAMAVER [39].

3. Results

3.1. X. citri has a set of conserved proteins in the Xanthomonas genus related to the uptake and assimilation of polyamines

X. citri potF gene (XAC2476) is in a cluster of 10 genes, separated from the putative putrescine ABC transporter components (PotIHG or XAC2470-2472) by three genes that respectively, encode an outer membrane protein (OprN) and two components of multidrug efflux pumps (RmrB and RmrA) (Fig. 1a). Upstream of *potF* sequence, we identified genes that encode enzymes related to putrescine biosynthesis, such as *bioA* (putrescine-pyruvate transaminase, XAC2477), *glnA* (glutamine synthetase, XAC2478), and *guaA* (glutamine amidotransferase, XAC2479). The putative ortholog of *X. citri* GlnA in *X. campestris,* XCC2346 protein, was identified in the proteome of extracellular extracts of the bacterium cultivated in minimum medium [40]. The genomic organization of polyamines-related genes in *P. aeruginosa* genome, reveals the absence of the multi-drug efflux pump genes and the presence of two genes encoding the periplasmic-binding proteins SpuD and SpuE that bind putrescine and spermidine, respectively [29]. These two proteins use the same ABC transport system SpuFGH. Differently, in *E. coli*, the genes encoding the components of putrescine (*potFGHI*) and polyamine (*potABCD*) transporters are in two separated operons (Fig. 1a). In *X. citri,* PotF is the periplasmic component of the PotGHI system, which specificity or affinity for polyamines are not known. A search for additional polyamine related proteins in the inner membrane of *X. citri* resulted in at least five putative systems: XAC2989 (PuuA/PuuP), an amino acid transporter (H^+) symporter, the proteins XAC3863/3864, XAC1841/1842 (YhdG) and XAC4354 (YhdG) forming three distinct cationic amino acid/polyamine antiporters, and the proteins XAC0856 to XAC0860 (Fig. 2). The latter was previously described as the components of an oligopeptide ABC transporter type importer [41], but in our search, these proteins also appear as orthologs of an *E. coli* ABC transporter dedicated to polyamines export, the SapBCDE system [42] (Fig. 1b) (Table S1, Supplementary material). In addition, we identified proteins in *X. citri* involved in polyamines biosynthesis and catalysis, as described in *E. coli* and *P. aeruginosa* [43–45]. Essentially, the enzymes belong to the anabolism of L-arginine to spermidine or putrescine and catabolism of putrescine to succinate (Fig. 2 and Table S1, Supplementary material). In the KEGG database, proteins XAC3923 (SpeA, arginine decarboxylase), XAC2302 (hypothetical), XAC2303 (N-carbamoylputrescine amidase), XAC3924 (SpeE, spermidine synthase), and XAC3002 (synthetase/amidase), are related to polyamine biosynthesis but their role in the bacterium is not clear. Considering that the *X. citri* polyamine transporter genes are found in a gene cluster with putrescine catabolism genes, it might suggest that this transporter is involved in acquiring putrescine as a carbon and nitrogen source.

3.2. The ligand-binding pocket of X. citri PotF conserves functional and structural characteristics for interaction with both putrescine and spermidine

To identify proteins that had structural similarity to *X. citri* PotF, its amino sequence was submitted to BLASTp against the Protein Data Bank. The search resulted in four spermidine/putrescine-binding

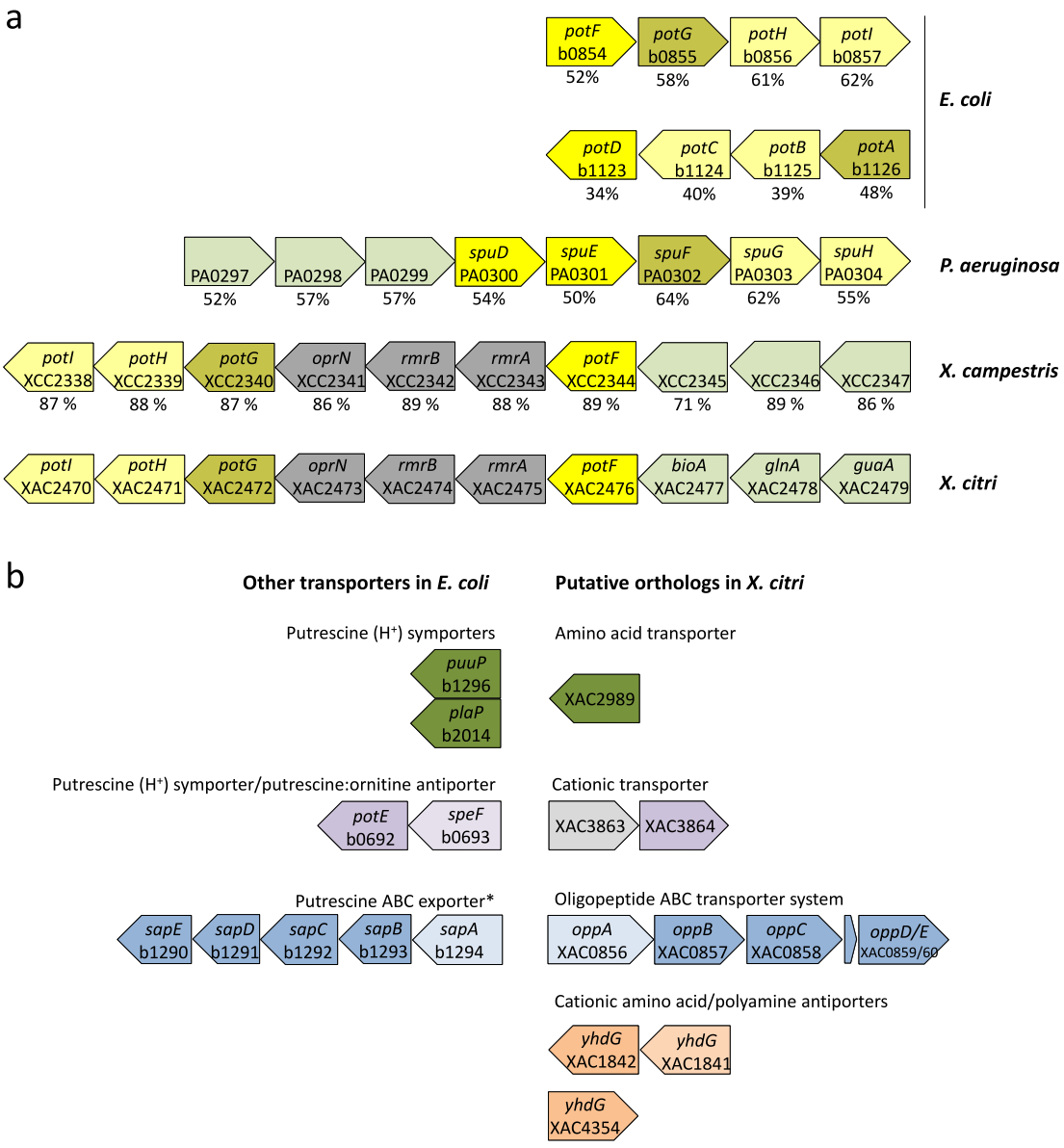

Fig. 1. Genetic organization of *pot* genes of *Xanthomonas citri* and related in comparison with *Xanthomonas campestris, Escherichia coli, and Pseudomonas aeruginosa.* (a) Cluster organization of Pot systems in *E. coli, P. aeruginosa, X. campestris* and *X. citri.* Yellow arrows represent genes from putative ABC transporter for putrescine/polyamine. KEGG codes and amino acid sequence identity is shown for each gene in comparison with *X. citri* ortholog. (b) Additional putrescine and polyamine transporter systems as described in *E coli* and their putative orthologs identified in *X. citri.* (*) *sapEDCB* operon is referred to as a putrescine ABC transporter type exporter, but *sapA* (b1294) gene encodes a periplasmic binding protein that usually belongs to importers. A list of all genes/proteins and their functions are presented in Table S1 (Supplementary material). (For interpretation of the references to colour in this figure legend, the reader is referred to the Web version of this article.)

proteins that shared more than 30% of amino acid sequence similarity with *X. citri* PotF: *E. coli* PotF bound to spermidine and putrescine (PDB codes 4JDF and 1A99, respectively), [27], *E. coli* PotD (monomer and dimer conformations, PDB codes 1POT and 1POY) [26], *P. aeruginosa* SpuD (apo and bound to putrescine, PDB codes 3TTK and 3TTM, respectively) and *P. aeruginosa* SpuE (apo and bound to spermidine, PDB codes 3TTL and 3TTN, respectively) [29] (Table S2, Supplementary material). For comparison with the putative orthologs, two three-dimensional models of PotF were built using the structural co-ordinates of *P. aeruginosa* SpuD and SpuE in bound states. These proteins shared 54% and 52% of amino acid sequence identity with the *X. citri* protein, respectively. To identify the ligand-binding pocket of *X. citri* PotF, the models were superimposed with the structures of *E. coli* and *P. aeruginosa* and analyzed together with the amino acid sequence alignment obtained with Clustal Omega program [28]. The sequential and structural alignment of the proteins showed conservation of the PotF binding pocket (Fig. 3a and b).

The four residues that promote polar interactions with putrescine in *E. coli* PotF and *P. aeruginosa* SpuD are conserved in *X. citri* PotF: S^{40}, D^{41} and D^{248}, and D^{279} (Fig. 3a). Similarly, the conservation is observed for residues that interact with spermidine (Fig. 3b), with exception of S^{343} (SpuE) and Q^{327} (PotD). In *X. citri* PotF, Y^{349} occupies the same position of S^{343} and Q^{327}. In addition, the presence of a set of aromatic residues that might help the stacking of the ligands is present in PotF's ligand-binding pocket. We also compared the electrostatic potential of the proteins and their pocket volumes (Fig. 4). In general, the proteins presented a similar charge distribution with an evident negative charge (red surface) in the pocket's entrance (yellow circle). Comparison of the

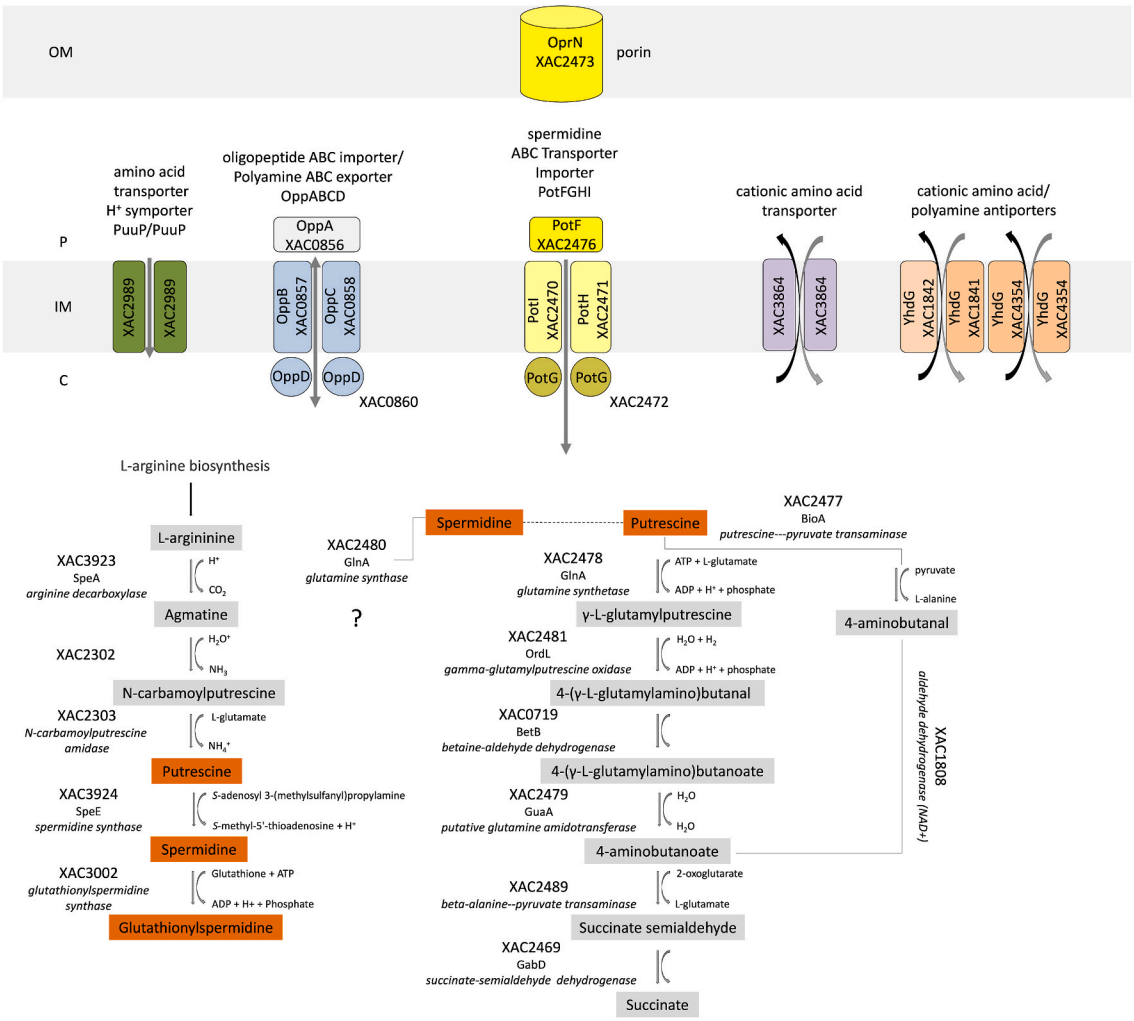

Fig. 2. General view of the putative systems for polyamines transport and related enzymes found in *Xanthomonas citri*. Proteins were identified using *E. coli* and *P. aeruginosa* orthologs described in the literature and search for keywords [polyamines], [spermine], [spermidine], and [putrescine] in *X. citri* databank (NCBI Reference sequence NC_003919.1). The pathways are shown as described for orthologs and in the Uniprot databank (https://www.uniprot.org). (?) enzymes missing or not identified, (P) periplasm, (IM) inner membrane, and (C) cytoplasm. *X. citri* enzymes are shown according to the KEGG reference. In gray boxes we show the intermediates compounds for each pathway. The list of all proteins, their putative functions, amino acid sequence identity, and orthologs for the search are described in Table S1 (Supplementary material).

PotF binding pocket with the other proteins revealed an elongated channel that could favour the interaction with spermidine (Fig. 4b, red surface). Altogether, the residues conservation, the surface charge, and shape of the pocket suggest the possibility of PotF interacting with both ligands, putrescine and spermidine.

3.3. *X. citri PotF was expressed as a soluble and stable protein and undergone structural changes in presence of both putrescine and spermidine*

To study the capability of *X. citri* PotF to bind spermidine and putrescine, a recombinant protein was produced in *E. coli* cells. After induction of *E. coli* Artic Express cells carrying the pET28-*potF* plasmid, soluble and stable PotF was expressed with an expected molecular mass of 38.2 kDa (Fig. S1, Supplementary material). The protein was purified using immobilized metal affinity chromatography (IMAC) and eluted with a 150 mM imidazole linear gradient. The purified samples were still submitted to the size-exclusion chromatography revealing one unique peak. After thrombin cleavage and size-exclusion chromatography steps, it was possible to obtain 5 mg of recombinant PotF per liter of culture. Dynamic light scattering analysis of PotF in the absence or presence of spermidine and putrescine showed that samples were monodisperse (0.2 polydispersity) consisting of a protein of estimated molecular weight of 37 kDa, which was compatible with its monomeric state (38.2 kDa). The hydrodynamic radius of the apo PotF was 3.37 nm and revealed a slight increase in presence of putrescine (3.43 nm) and spermidine (3.53 nm) (Fig. S1,Supplementary material).

The samples were submitted to circular dichroism (CD) analysis (Fig. 5). The CD spectrum of apo PotF was characteristic of an α/β protein, as expected from the bioinformatics analyses and structural model, with minima signals at 208 nm and 222 nm. The presence of putrescine or spermidine in the samples slightly altered the secondary structure content and profile of the protein (Fig. 5a). The PotF's thermal stability also was evaluated in apo-state and in the presence of the putative ligands. Samples were evaluated before (20 °C) and after incubation of the protein at 100 °C. The spectrum of the protein submitted to high temperature revealed the loss of the peak at 222 nm and decreasing in the α-helices content (Fig. 5b, dashed line) when compared to the protein at 20 °C (solid line). A slight increase of this peak is observed in the profile of the protein submitted to decreasing of the temperature (100 °C–20 °C) (Fig. 5b, dot line). Although PotF showed loss of secondary structure content with increasing of temperature, it did not undergo complete denaturation, as observed by the CD values. To determinate the temperature of melting (T_m) and influence of the

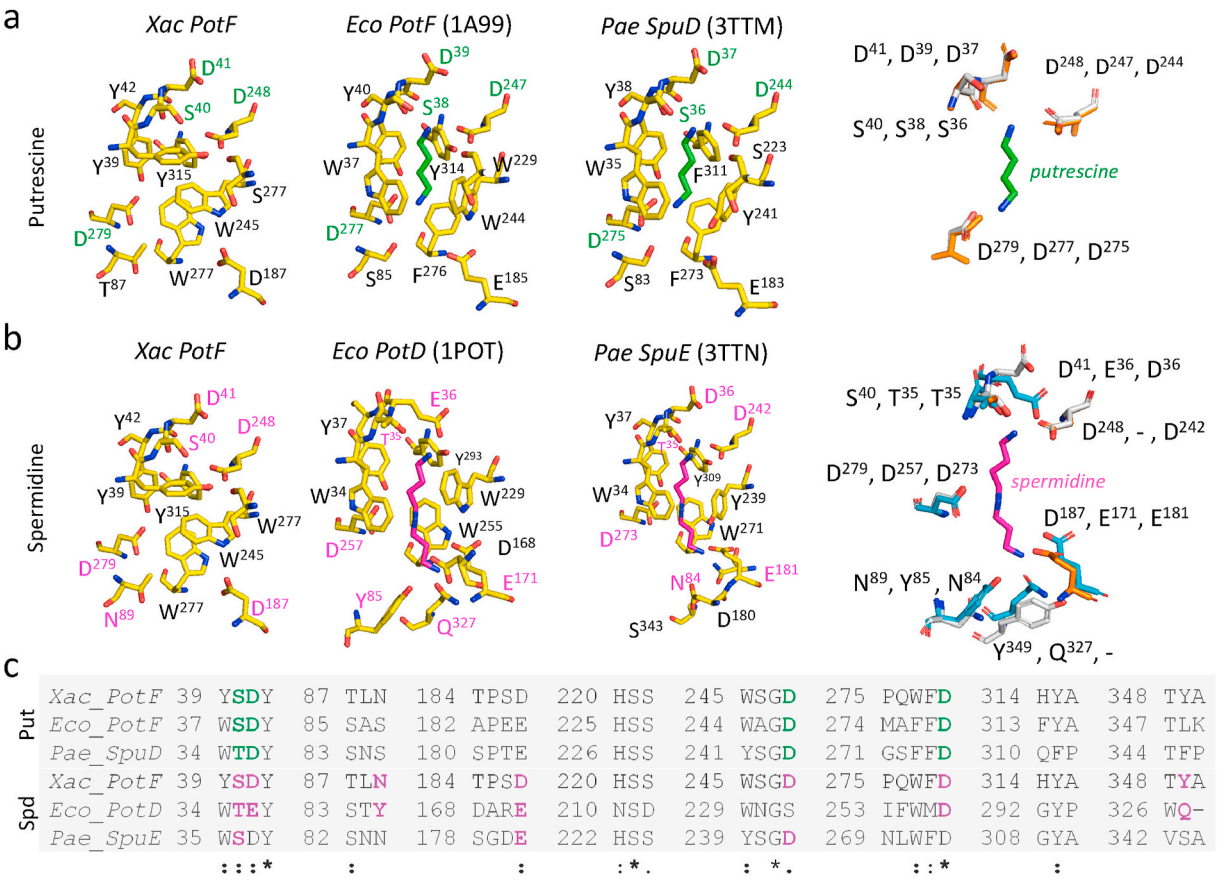

Fig. 3. The *Xanthomonas citri* PotF ligand-binding pocket in comparison with orthologs that have three-dimensional structures available. (a) Comparison of *X. citri* PotF with *E. coli* (PotF) and *P. aeruginosa* (SpuD) putrescine-binding proteins. (b) PotF in comparison with *E. coli* (PotD) and *P. aeruginosa* (SpuE) spermidine-binding proteins. Residues from the pocket of each protein are shown in yellow stick and those that interact with putrescine and spermidine are shown in green and pink, respectively. (c) Structure-based amino acid sequence alignment of the polyamine-binding proteins. The alignment was performed using Clustal Omega Multiple Sequence Alignment program [28] and highlights the residues involved with polyamines binding (in coloured bold). The numbers are described according to the protein structures. Conservation of residues is shown as: (*) identical; (:) similar; (.) different. Xac_PotF: KEGG reference Xac2476, Eco_PotF: *E. coli* putrescine-binding protein PotF bound to putrescine (PDB code 1A99) [27]; Pae_SpuD: *P. aeruginosa* putrescine-binding protein SpuD bound to putrescine (PDB code 3TTM) [29]; Eco_PotD: *E. coli* spermidine/putrescine-binding protein PotD bound to spermidine (PDB code 1POT) [26]; Pae_SpuE: *P. aeruginosa* spermidine-binding protein SpuE bound to spermidine (PDB code 3TTN) [29]. (For interpretation of the references to colour in this figure legend, the reader is referred to the Web version of this article.)

polyamines, PotF was submitted to the thermal denaturation analysis in the absence and presence of 50 μM of putrescine and spermidine. The results revealed that the T_m of PotF, which was 61 °C, was not significantly changed in presence of putrescine and remained around 63 °C ± 2 °C but undergone a significant increase of 5° after spermidine addition (T_m = 68 °C) (Fig. 5c). Thermal shift analysis of PotF with increasing concentrations of the ligands corroborated the previous results and indicated that spermidine significantly induced the protein thermal stability (Fig. 5d).

3.4. PotF binds both putrescine and spermidine

X. citri PotF has an intrinsic fluorescence due to the presence of aromatic amino acid residues. Specifically, PotF has four tryptophans (Fig. 6a), including two very close to the ligand-binding site (W^{245} and W^{277}) that allowed us to monitor the variations in the intrinsic fluorescence upon titration with putrescine and spermidine (Fig. 6b and c). Fluorescence experiments were performed using 1 ml samples of PotF (9 μM) in buffer solution 50 mM Tris-HCl pH 8.0 and 50 mM NaCl and a stock solution of putrescine or spermidine (1 mM) in the same buffer solution. The emission spectra were obtained at 22.5 °C using an excitation beam light at 295 nm. Fig. 6b displays PotF fluorescence spectra in buffer with increasing amounts of putrescine. The fluorescence quantum yield is the ratio between the number of photons emitted and absorbed. Once that interaction of PotF with putrescine did not change its absorption spectra, it becomes evident that the interaction with this polyamine increased the fluorescence quantum yield. As there are no changes in the position of the fluorescent band (see Fig. 6b), the fraction of the fluorescence intensity changes at its maximum, 340 nm, [$\Delta F/\Delta F_{max} = (F–F_0)/(F\text{-}F_{max})$], and is plotted as a function of the putrescine concentration (Fig. 6d). F_0, F, and F_{max} are the fluorescence intensities of PotF at 340 nm in the absence of ligand, at a given ligand concentration, and at saturating concentration, respectively. By using eq. (1) (Experimental procedures) to fit the experimental results, the binding constant (K_b) was determined as 1.7×10^5 M^{-1} (K_d = 5.9 μM) (Fig. 6d).

Similarly, the behaviour of PotF in the presence of spermidine was evaluated (Fig. 6c and e). Spermidine also did not change significantly the PotF fluorescence absorption spectrum. However, different from putrescine, increasing the concentration of spermidine not only increased the protein fluorescence intensity but also caused a blue shift in its emission spectrum (Fig. 6c). Under saturated conditions, the position of the maximum emission shifts 15 nm, from 340 to 325 nm. It is interesting to point out that the change in the PotF fluorescence spectrum saturates when spermidine concentration (5.9 μM) is smaller than that of PotF (9 μM). This could indicate that during the different processes of PotF production some molecules ended up not presenting free

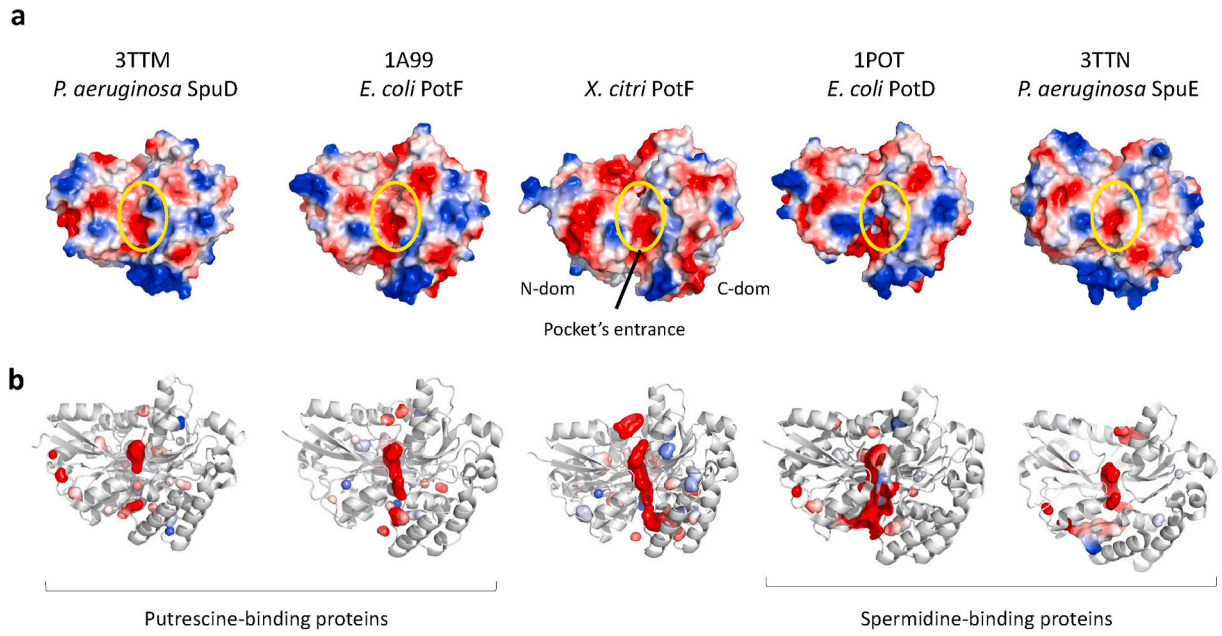

Fig. 4. Electrostatic potential and volume of the pockets in polyamine binding proteins in comparison with *Xanthomonas citri* PotF. (a) Comparison of the surface electrostatic potential from *X. citri* PotF and the polyamine binding proteins. The figure shows the proteins from the pocket (black circle) entrance perspective, detaching N- and C-domains. Electrostatic potential is shown as red, blue, and gray for negative, positive, and neutral charges, respectively. (b) Differences in the pocket of the five proteins. The pocket inner volumes are detached as red surfaces in the cartoon representation of the proteins. PDBs used for calculation are shown above the name of the proteins. (For interpretation of the references to colour in this figure legend, the reader is referred to the Web version of this article.)

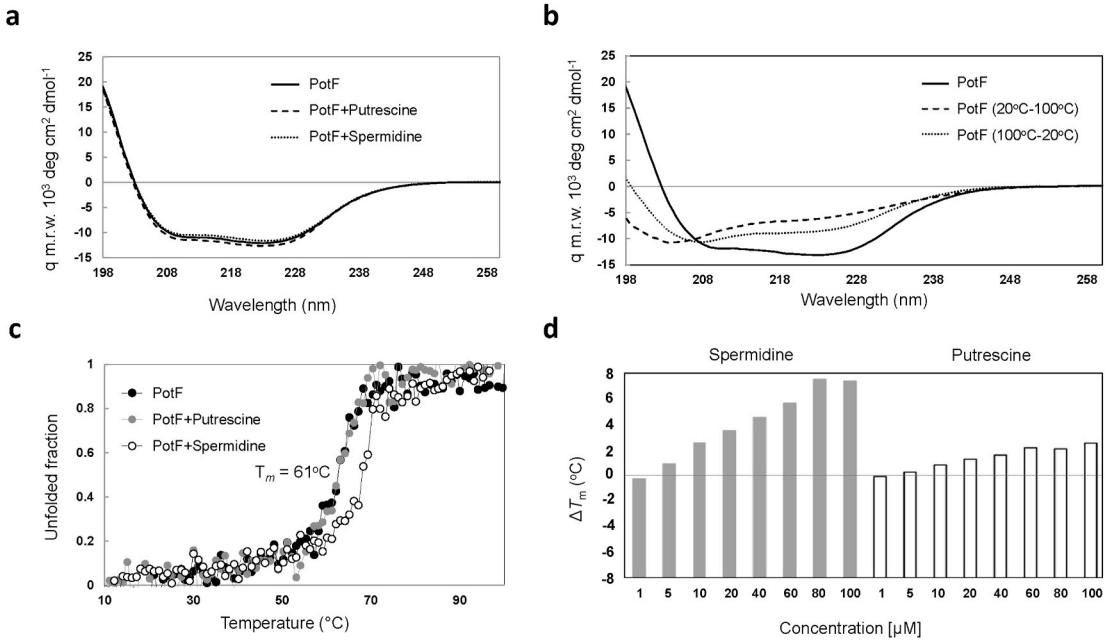

Fig. 5. Circular dichroism analysis of *Xanthomonas citri* PotF. (a) CD spectra of PotF (solid line) in comparison with PotF + 30 μM putrescine (dashed line) and PotF + 30 μM spermidine (dotted line). (b) CD spectra of the recombinant PotF (solid line) at 20 °C, after the increasing of the temperature up to 100 °C (dashed line) and after the decreasing of the temperature back to 20 °C (dotted line). (c) Thermal-induced unfolding of PotF (●), PotF + 50 μM of putrescine (●), and PotF + 50 μM of spermidine (○). Unfolding was followed by measuring the ellipticity at 222 nm during increasing of the temperature from 10 °C to 100 °C, with 0.5 °C of intervals between each spectrum acquisition. (d) Thermal shift assay of PotF in presence of polyamines. Bar graph illustrates shifts of T_m for an increased concentration of polyamines. CD spectra were acquired with 3 μM of protein in 10 mM sodium phosphate buffer pH 7.4 and 10 mM NaCl as described in Experimental procedures.

spermidine binding site. Considering the shift in the fluorescent spectrum, the graphic of the fraction of the fluorescence change, $\Delta F/\Delta F_{max}$, versus the spermidine concentration (Fig. 6e), used the fluorescence at 325 nm, which is the maximum of the fluorescent band at saturated spermidine concentration. It is important to mention that when the affinity is large, i. e., $K_bC_{PotF} \gg 1$, the determination of K_b is inaccurate because the titration curve (Fig. 6e) is composed by nearly two straight lines [32]. Then, we determined the value of K_b as the lower limit for the binding constant, therefore $K_b \geq 5.0 \times 10^8\ M^{-1}$ ($K_d \leq 2$ nM). It is noteworthy that a higher K_b value fits the experimental data (Fig. S2,

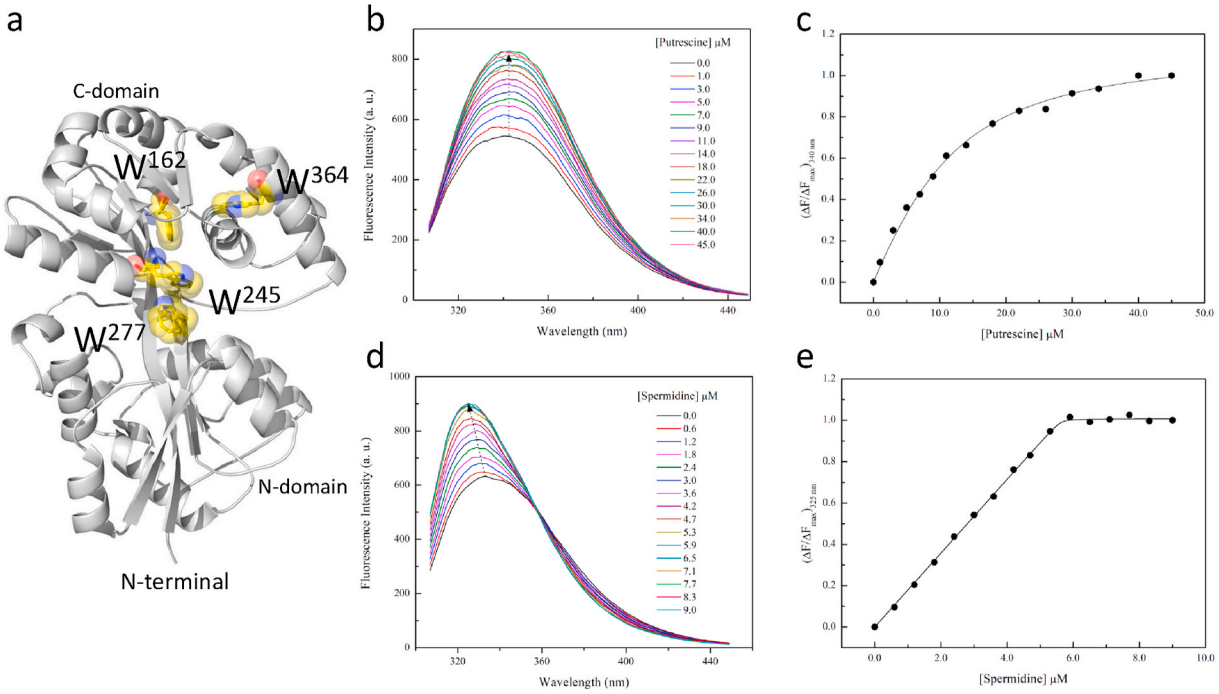

Fig. 6. Intrinsic fluorescence measurements of *Xanthomonas citri* PotF. (a) Three-dimensional structure model of PotF in cartoon showing the position of the four residues of tryptophans (showed as balls) identified in the protein sequence. Putrescine and spermidine (cyan and pink sticks, respectively) were docked in the ligand-binding pocket to show the proximity with the tryptophans. Domains N- and C are pointed. (b) Typical fluorescence spectra of 9 μM PotF (in buffer 50 mM Tris pH 8.0 and 50 mM NaCl) in the absence and with increasing concentration of putrescine. (c) Normalized change of PotF fluorescence at 340 nm as a function of putrescine concentration. (d) Typical fluorescence spectra 9 μM PotF (in buffer 50 mM Tris pH 8.0 and 50 mM NaCl) in the absence and with increasing concentration of spermidine. (e) Normalized change of PotF fluorescence at 325 nm as a function of spermidine concentration. If not shown, the error bar was found to be smaller than the symbol. Excitation wavelength at 295 nm. (For interpretation of the references to colour in this figure legend, the reader is referred to the Web version of this article.)

Supplementary material).

3.5. Small-angle X-ray scattering (SAXS) analysis of PotF in presence of putrescine and spermidine

In order to investigate PotF structural conformation in the apo and in the presence of 300 μM of putrescine or spermidine, we performed SAXS measurements. The SAXS data fit was computed by GNOM program [34] assuming a monodisperse system (Fig. 7a), and the evaluated pair distribution functions, p(r), are shown in Fig. 7b for each analyzed sample. The p(r) function showed similar behavior in the three SAXS profiles, where a bell shape was obtained with a maximum at 25 Å and a maximum dimension within the particle (D_{max}) of approximately 73 Å. Low-resolution models were obtained using the program DAMMIN [37]. From the Kratky Plot ($I.q^2$ vs. q) analysis we obtained information related to protein flexibility (Fig. 7c). In this plot, compact samples may present a bell shape with the curve approaching zero at high q values. Any degree of internal flexibility may cause an increase in the final region. As it can be seen, the samples presented similar behavior, indicating a globular compact folded particle. The average model from 10 independent runs to each SAXS data showed a prolate shape where it was observed a slightly more compact arrangement in the case of PotF in the presence of spermidine (Fig. 7d). The samples also presented similar structural parameters of radius of gyration (R_g) (PotF: $R_g = 22.0 \pm 0.1$ Å; PotF + Putrescine: $R_g = 21.9 \pm 0.1$ Å; PotF + Spermidine: $R_g = 21.8 \pm 0.1$ Å), derived from GNOM.

In an attempt to compare experimental SAXS data collected for PotF and theoretical SAXS intensity calculated from the high-resolution 3D models, we used CRYSOL program [35] and the structural coordinates of *P. aeruginosa* SpuD (PDB 3TTM) as an entry (Table S2, Supplementary Information). The superposition of the calculated (3TTM) and experimental SAXS profiles (PotF-apo and in the presence of ligands) are shown in Fig. 8a as well as the determined *ab initio* structural models in comparison with the 3TTM structure Fig. 8b. The results indicated that the crystal model 3TTM was able to describe the SAXS data for the native protein and the sample with ligands, with a slightly better agreement for the protein in the presence of putrescine ($\chi^2 = 4.0$).

4. Discussion

Polyamines are important molecules found in all living organisms, including plants, where they play several physiological functions from embryogenesis to flowering [46]. *X. citri* is a phytopathogenic bacterium that infects citrus plants, but little is known about the role of polyamines during the infection process. The citrus canker disease has no treatment and the knowledge of the essential mechanisms that the bacterium uses for infection, virulence, and pathogenesis are important steps for the development of forms of disease control. In this work, we seek to characterize the set of genes and corresponding proteins dedicated to polyamine biosynthesis, catabolism and transport in *X. citri* and highlight the structural and mechanistic characterization of the PotF protein. Moreover, we compared the genomic organization of polyamine-related genes in *Xanthomonas* species and other gamma-proteobacteria. Despite the differences found in the genetic organization, PotF is highly conserved in other species of *Xanthomonas* genus, with amino acid sequence identities higher than 71%, indicating the functional conservation and relevance of these proteins for bacteria that infect plants during the evolution. The presence of one bivalent operon instead of two, revealed a greater use of the genome in *X. citri* than in *E. coli* or *P. aeruginosa*.

X. citri PotF showed capability to interact with not only one, but two polyamines, putrescine, and spermidine. The comparison of the ligand-

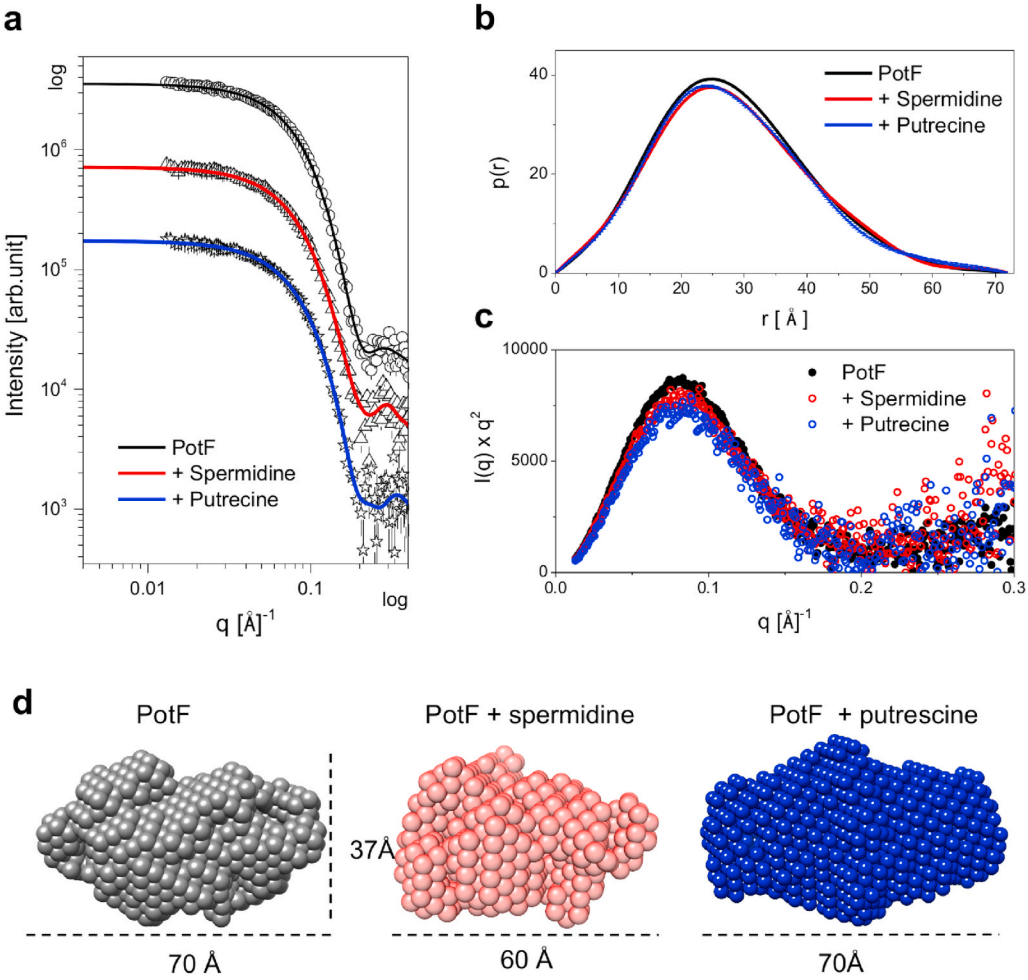

Fig. 7. SAXS data analysis for *X. citri* apo PotF and in presence of putrescine and spermidine. (a) Experimental SAXS profile of PotF, PotF + putrescine, and PotF + spermidine and the fitting obtained using the GNOM program with IFT method assuming a monodisperse system. (b) The pair-distance distribution function p(r) respectively for each analyzed SAXS profile in (a). (c) Kratky plot obtained by $I(q)xq^2$ versus q for apo PotF and PotF in presence of putrescine and spermidine. (d) *Ab initio* models using DAMMIN program for apo PotF (gray) and PotF in presence of spermidine (red) and putrescine (blue), the average envelopes for ten individual runs, respectively for each sample, are shown in sphere representation. The models show a slightly compact conformation for PotF in the presence of spermidine. (For interpretation of the references to colour in this figure legend, the reader is referred to the Web version of this article.)

binding site of *X. citri* PotF with spermidine-binding proteins of *P. aeruginosa* (SpuE) and *E. coli* (PotD) revealed the presence of W^{277} in a key position. Wu and co-workers [29] showed that the presence of this amino acid is essential for differentiation between spermidine or putrescine binding. This comparison suggested that *X. citri* PotF could bind spermidine but not putrescine. Indeed, our further experiments evidenced that PotF prefers spermidine, but also binds putrescine. The binding affinities and the effects of the ligand interaction were also evaluated in biophysical assays that showed more significant changes of the protein in the presence of spermidine than putrescine, including higher thermal stability. That might be explained by the fact that spermidine is twice the size of putrescine, which would lead to a higher occupancy of the ligand-binding site and interactions with residues. Fluorescence experiments showed that both polyamines changed the emission of PotF, increasing the fluorescence quantum yield indicating that the non-radiative decay processes decrease in the ligand-bound protein. Interestingly, this could be interpreted as an increase in the rigidity of the environment of the tryptophan, since it is already well established that the increase in the rigidity can enhance the fluorescence quantum yield [31]. The interaction with putrescine did not shift the PotF emission spectrum (Fig. 6b), indicating that the region of the tryptophan residues is not changing in terms of accessibility to the molecules of the solvent. In contrast, the interaction between PotF and spermidine shifts the emission spectra to about −15 nm (Fig. 6d). This is an indication that tryptophan dipolar relaxation is decreasing, suggesting a change in PotF conformation where tryptophan residues would sense a more hydrophobic environment. This result is related to the larger size of spermidine in comparison with putrescine and its occupancy in the ligand-binding site, facing W^{245} and W^{277} residues.

SAXS data showed similar behaviour for PotF in the apo and in the presence of both ligands and suggested that PotF in the presence of spermidine acquired a slightly more compact arrangement than the apo PotF. The crystal model 3TTM was able to describe the experimental SAXS profile in a reasonable agreement in all cases, with indicated that the overall shape of the high-resolution structure for the protein, especially in the presence of putrescine where a slightly better fit was obtained.

The physiological relevance of this observation is important since both putrescine and spermidine are abundant polyamines present in citrus plants. In *Citrus sinensis*, nanomolar concentrations of polyamines are observed in the leaves, with a higher range of spermidine (180–220 nmol/g) than putrescine (40–80 nmol/g) [47]. These differences of polyamine concentration in plant tissues that *X. citri* infect, could explain why *X. citri* PotF showed higher affinity by spermidine than putrescine. On the other hand, based upon the binding constant for putrescine reported in the work, on the set of proteins related to putrescine metabolism, and the expected putrescine's concentration in vivo, is it realistic to expect that *X. citri* PotF also can function as a putrescine transporter. It is important to note that the ability of the phytopathogen to capture and use host polyamines in its metabolism should affect the plant performance and increase the virulence and pathogenesis of the phytopathogen. It would be interesting to characterize the polyamines transport in vivo, using mutant strains. NspS, a homologue of ABC-type periplasmic solute binding proteins identified in *Vibrio cholerae,* facilitates transduction of polyamine binding signals independent of their transport [48].

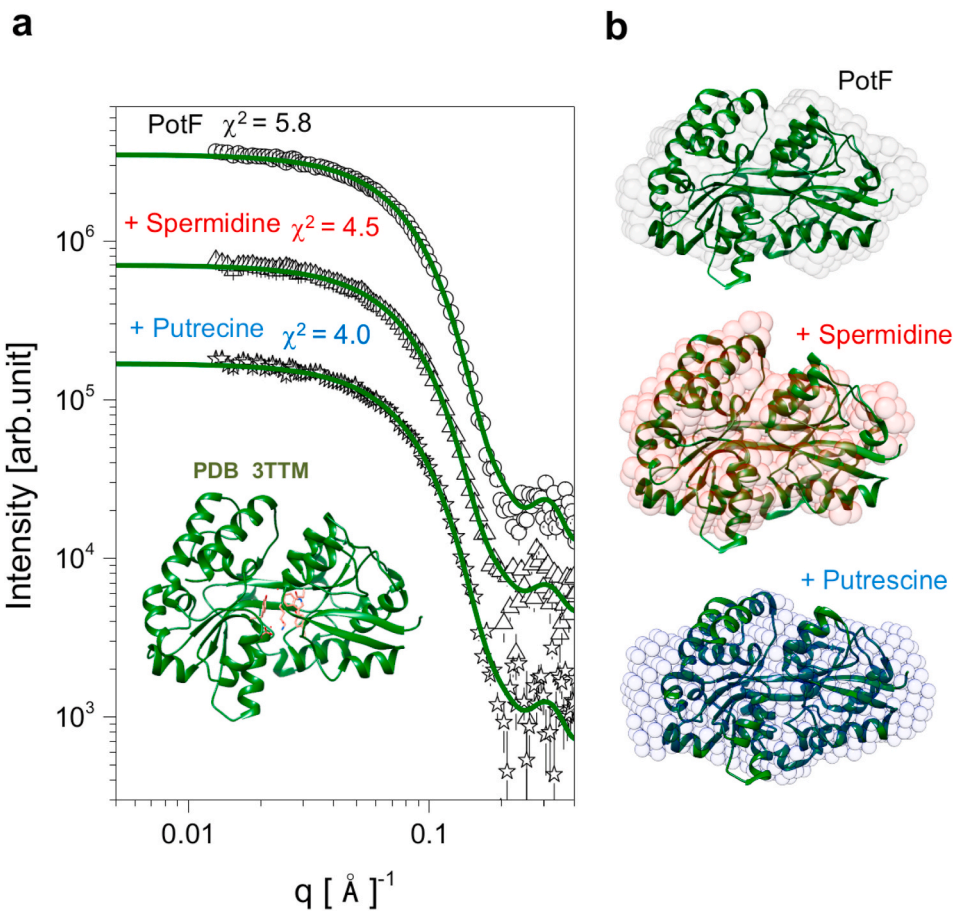

Fig. 8. Comparison of the SAXS experimental data to the crystal model 3TTM. (a) Superposition of the experimental intensity of SAXS measured for apo PotF (up), PotF + spermidine (middle) and PotF + putrescine(down)with the theoretical SASX profile for 3TTM model (inset plot as green *cartoon* representation), resulting in a χ^2 of 5.8, 4.5 and 3.7, respectively. (b) Comparison between Ab initio models and 3TTM for apo PotF (up), PotF + spermidine (middle) and PotF + putrescine (down). (For interpretation of the references to colour in this figure legend, the reader is referred to the Web version of this article.)

5. Conclusions

Altogether, the data presented in this work showed that *X. citri* presents a set of conserved proteins in *Xanthomonas* genus that are dedicated to the polyamine metabolism and transport. PotF, the periplasmic component of the ABC transport system, is a dual spermidine/putrescine-binding protein that showed higher affinity for spermidine than putrescine. The evident preference of PotF for spermidine suggests this polyamine might plays an important role during the process of infection and pathogenesis of the bacterium and highlights the need for further genetic studies. Moreover, the data reveals that PotF could be an important target for development of specific inhibitors, since it is highly conserved and localized in the periplasm, with easy access to external environment.

Author contributions

Aline Sampaio Cremonesi: investigation, writing-original draft preparation; Lilia I. De la Torre: investigation and fluorescence data; Maximillia Frazão de Souza: writing and SAXS data analysis; Gabriel S. Vignoli Muniz: investigation, fluorescence data analysis; Maria Teresa Lamy: conceptualization, fluorescence analysis; Cristiano Luis Pinto Oliveira: SAXS experiments, conceptualization, and data analysis; Andrea Balan: supervision, writing-reviewing, and editing.

Funding and additional information

This work was supported by Fundação de Amparo à Pesquisa do Estado de São Paulo (FAPESP), grant numbers 2011/22386-2 (PhD fellowship for ASP), 2018/20162-9 (Regular Research Project); Conselho Nacional de Desenvolvimento Científico (CNPq), grant number 401505/2016-2 (Universal Research Project); Coordenação de Aperfeiçoamento de Pessoal de Nível Superior (CAPES); COLCIENCIAS (PhD fellowship for LILT). MTL is recipient of CNPq research fellowships. GSVM and MTL are part of the National Institute of Science and Technology Complex Fluids (INCT-FCx), financed by CNPq (465259/2014-6) and FAPESP (2014/50983-3).

Declaration of competing interest

The authors declare that they have no conflicts of interest with the contents of this article.

Acknowledgements

We thank the infrastructure offered by the Brazilian National Laboratory of Synchrotron Light (LNLS), Campinas, Brazil, and the Department of Experimental Physics, University of São Paulo. The authors are pleased to thank Dr. Sonia R. W. Louro for important discussions.

Abbreviations - The abbreviations used are:

K_d	dissociation constant
DLS	dynamic light scattering
D_{max}	maximum diameter
DTT	dithiothreitol
FPLC	fast protein liquid chromatography
IPTG	isopropyl β-D-1-thiogalactopyranoside
KEGG	Kyoto Encyclopedia of Genes and Genomes database
K_b	binding constant
p(r)	pair distribution function
PDB	protein data bank

PMSF	phenylmethylsulfonyl fluoride
R_g	radius of gyration
SAXS	small-angle X-ray scattering
T_m	temperature of melting
X. citri	Xanthomonas citri

Appendix A. Supplementary data

Supplementary data to this article can be found online at https://doi.org/10.1016/j.bbrep.2021.101171.

References

[1] A.M. Brunings, D.W. Gabriel, *Xanthomonas citri*: breaking the surface, Mol. Plant Pathol. 4 (2003) 141–157, https://doi.org/10.1046/j.1364-3703.2003.00163.x.

[2] M. Nitschke, V. Rodrigues, Effect of virulence and serial transfers of *Xanthomonas campestris* on xanthan gum production, Braz. J. Microbiol. 31 (2000) 58–60, https://doi.org/10.1590/S1517-83822000000100014.

[3] A.A. Vojnov, A. Zorreguieta, J.M. Dow, M.J. Daniels, M.A. Dankert, Evidence for a role for the *gumB* and *gumC* gene products in the formation of xanthan from its pentasaccharide repeating unit by *Xanthomonas campestris*, Microbiology 144 (1998) 1487–1493, https://doi.org/10.1099/00221287-144-6-1487.

[4] R.P. Ryan, F.J. Vorhölter, N. Potnis, J.B. Jones, M.A. Van Sluys, A.J. Bogdanove, J. M. Dow, Pathogenomics of *Xanthomonas*: understanding bacterium-plant interactions, Nat. Rev. Microbiol. 9 (2011) 344–355, https://doi.org/10.1038/nrmicro2558.

[5] N. Mhedbi-Hajri, A. Darrasse, S. Pigné, K. Durand, S. Fouteau, V. Barbe, C. Manceau, C. Lemaire, M.A. Jacques, Sensing and adhesion are adaptive functions in the plant pathogenic xanthomonads, BMC Evol. Biol. 11 (2011), https://doi.org/10.1186/1471-2148-11-67.

[6] D.P. Souza, G.U. Oka, C.E. Alvarez-Martinez, A.W. Bisson-Filho, G. Dunger, L. Hobeika, N.S. Cavalcante, M.C. Alegria, L.R.S. Barbosa, R.K. Salinas, C.R. Guzzo, C.S. Farah, Bacterial killing via a type IV secretion system, Nat. Commun. 6 (2015) 1–9, https://doi.org/10.1038/ncomms7453.

[7] G. Dunger, C.R. Guzzo, M.O. Andrade, J.B. Jones, C.S. Farah, *Xanthomonas citri* subsp. *citri* type IV pilus is required for twitching motility, biofilm development, and adherence, Mol. Plant Microbe Interact. 27 (2014) 1132–1147, https://doi.org/10.1094/MPMI-06-14-0184-R.

[8] E.E. Oshiro, M.B. Tavares, C.F. Suzuki, D.C. Pimenta, C.B. Angeli, J.C.F. de Oliveira, M.I.T. Ferro, L.C.S. Ferreira, R.C.C. Ferreira, Distribution and biological role of the oligopeptide-binding protein (OppA) in *Xanthomonas* species, Genet. Mol. Biol. 33 (2010) 341–347, https://doi.org/10.1590/S1415-47572010005000049.

[9] A. Casabuono, S. Petrocelli, J. Ottado, E.G. Orellano, A.S. Couto, Structural analysis and involvement in plant innate immunity of *Xanthomonas axonopodis* pv. *citri* lipopolysaccharide, J. Biol. Chem. 286 (2011) 25628–25643, https://doi.org/10.1074/jbc.M110.186049.

[10] F. Tófoli De Araújo, V.M. Bolanos-Garcia, C.T. Pereira, M. Sanches, E.E. Oshiro, R. C.C. Ferreira, D.Y. Chigardze, J.A. Gonçalves Barbosa, L.C.D.S. Ferreira, C. E. Benedetti, T.L. Blundell, A. Balan, Structural and physiological analyses of the alkanesulphonate-binding protein (SsuA) of the citrus pathogen *Xanthomonas citri*, PLoS One 8 (2013), https://doi.org/10.1371/journal.pone.0080083.

[11] V.R. Pegos, J.F. Nascimento, T.J.P. Sobreira, B.A. Pauletti, A. Paes-Leme, A. Balan, Phosphate regulated proteins of *Xanthomonas citri* subsp. *citri*: a proteomic approach, J. Proteomics. 108 (2014) 78–88, https://doi.org/10.1016/j.jprot.2014.05.005.

[12] L.M. Moreira, A.P. Facincani, C.B. Ferreira, R.M. Ferreira, M.I.T. Ferro, F.C. Gozzo, J.C.F. de Oliveira, J.A. Ferro, M.R. Soares, Chemotactic signal transduction and phosphate metabolism as adaptive strategies during citrus canker induction by *Xanthomonas citri*, Funct. Integr. Genom. 15 (2015) 197–210, https://doi.org/10.1007/s10142-014-0414-z.

[13] Q. Yan, N. Wang, High-throughput screening and analysis of genes of *Xanthomonas citri* subsp. *citri* involved in citrus canker symptom development, Mol. Plant Microbe Interact. 25 (2012) 69–84, https://doi.org/10.1094/MPMI-05-11-0121.

[14] A. Mehta, Y.B. Rosato, Identification of differentially expressed genes of *Xanthomonas axonopodis* pv. *citri* by representational difference analysis of cDNA, Genet. Mol. Biol. 28 (2005) 140–149, https://doi.org/10.1590/S1415-47572005000100024.

[15] M.R. Soares, A.P. Facincani, R.M. Ferreira, L.M. Moreira, J.C.F. de Oliveira, J. A. Ferro, M.I.T. Ferro, R. Meneghini, F.C. Gozzo, Proteome of the phytopathogen *Xanthomonas citri* subsp. *citri*: a global expression profile, Proteome Sci. 8 (2010) 1–11, https://doi.org/10.1186/1477-5956-8-55.

[16] K. Igarashi, K. Kashiwagi, The functional role of polyamines in eukaryotic cells, Int. J. Biochem. Cell Biol. 107 (2019) 104–115, https://doi.org/10.1016/j.biocel.2018.12.012.

[17] A.J. Michael, Polyamine function in archaea and bacteria, J. Biol. Chem. 293 (2018) 18693–18701, https://doi.org/10.1074/jbc.TM118.005670.

[18] K. Igarashi, K. Kashiwagi, Polyamines: mysterious modulators of cellular functions, Biochem. Biophys. Res. Commun. 271 (2000) 559–564, https://doi.org/10.1006/bbrc.2000.2601.

[19] C.W. Tabor, H. Tabor, Polyamines in microorganisms, Microbiol. Rev. 49 (1985) 81–99, https://doi.org/10.1128/mmbr.49.1.81-99.1985.

[20] D.H. Bae, D.J.R. Lane, P.J. Jansson, D.R. Richardson, The old and new biochemistry of polyamines, Biochim. Biophys. Acta Gen. Subj. 1862 (2018) 2053–2068, https://doi.org/10.1016/j.bbagen.2018.06.004.

[21] M.A. Phillips, Polyamines in protozoan pathogens, J. Biol. Chem. 293 (2018) 18746–18756, https://doi.org/10.1074/jbc.TM118.003342.

[22] C. Martini, C. Michaux, F. Bugli, A. Arcovito, F. Iavarone, M. Cacaci, F.P. Sterbini, A. Hartke, N. Sauvageot, M. Sanguinetti, B. Posteraro, J.C. Giard, The polyamine N-acetyltransferase-like enzyme PmvE plays a role in the virulence of Enterococcus faecalis, Infect. Immun. 83 (2015) 364–371, https://doi.org/10.1128/IAI.02585-14.

[23] W. Wojtasik, A. Kulma, K. Namysł, M. Preisner, J. Szopa, Polyamine metabolism in flax in response to treatment with pathogenic and non–pathogenic Fusarium strains, Front. Plant Sci. 6 (2015) 1–12, https://doi.org/10.3389/fpls.2015.00291.

[24] L. Zhou, J. Wang, L.H. Zhang, Modulation of bacterial type III secretion system by a spermidine transporter dependent signaling pathway, PLoS One 2 (2007), https://doi.org/10.1371/journal.pone.0001291.

[25] Y. Terui, S.D. Saroj, A. Sakamoto, T. Yoshida, K. Higashi, S. Kurihara, H. Suzuki, T. Toida, K. Kashiwagi, K. Igarashi, Properties of putrescine uptake by PotFGHI and PuuP and their physiological significance in *Escherichia coli*, Amino Acids 46 (2014) 661–670, https://doi.org/10.1007/s00726-013-1517-x.

[26] S. Sugiyama, Y. Matsuo, K. Maenaka, D.G. Vassylyev, M. Matsushima, K. Kashiwagi, K. Igarashi, K. Morikawa, The 1.8-Å X-ray structure of the *Escherichia coli* PotD protein complexed with spermidine and the mechanism of polyamine binding, Protein Sci. 5 (1996) 1984–1990, https://doi.org/10.1002/pro.5560051004.

[27] D.G. Vassylyev, H. Tomitori, K. Kashiwagi, K. Morikawa, K. Igarashi, Crystal structure and mutational analysis of the *Escherichia coli* putrescine receptor. Structural basis for substrate specificity, J. Biol. Chem. 273 (1998) 17604–17609, https://doi.org/10.1074/jbc.273.28.17604.

[28] F. Sievers, A. Wilm, D. Dineen, T.J. Gibson, K. Karplus, W. Li, R. Lopez, H. McWilliam, M. Remmert, J. Söding, J.D. Thompson, D.G. Higgins, Fast, scalable generation of high-quality protein multiple sequence alignments using Clustal Omega, Mol. Syst. Biol. 7 (2011), https://doi.org/10.1038/msb.2011.75.

[29] D. Wu, S.C. Lim, Y. Dong, J. Wu, F. Tao, L. Zhou, L.H. Zhang, H. Song, Structural basis of substrate binding specificity revealed by the crystal structures of polyamine receptors SpuD and SpuE from *Pseudomonas aeruginosa*, J. Mol. Biol. 416 (2012) 697–712, https://doi.org/10.1016/j.jmb.2012.01.010.

[30] J. Sambrook, Cold Spring Harbor, in: Molecular Cloning : a Laboratory Manual, third ed., Cold Spring Harbor Laboratory Press, N.Y., 2001. n.d. https://search.library.wisc.edu/catalog/999897924602121.

[31] J.R. Lakowicz, Principles of Fluorescence Spectroscopy, second ed., Kluwer Academic/Plenum, New York, 1999. ©1999, n.d, https://search.library.wisc.edu/catalog/999882542202121.

[32] B. Valeur, Molecular Fluorescence: Principles and Applications, Wiley-VCH, Weinheim, New York, 2002.

[33] A.P. Hammersley, FIT2D: a multi-purpose data reduction, analysis and visualization program, J. Appl. Crystallogr. 49 (2016) 646–652, https://doi.org/10.1107/S1600576716000455.

[34] A.V. Semenyuk, D.I. Svergun, GNOM. A program package for small-angle scattering data processing, J. Appl. Crystallogr. 24 (1991) 537–540, https://doi.org/10.1107/S002188989100081X.

[35] D. Svergun, C. Barberato, M.H. Koch, CRYSOL - a program to evaluate X-ray solution scattering of biological macromolecules from atomic coordinates, J. Appl. Crystallogr. 28 (1995) 768–773, https://doi.org/10.1107/S0021889895007047.

[36] M.V. Petoukhov, D. Franke, A.V. Shkumatov, G. Tria, A.G. Kikhney, M. Gajda, C. Gorba, H.D.T. Mertens, P.V. Konarev, D.I. Svergun, New developments in the ATSAS program package for small-angle scattering data analysis, J. Appl. Crystallogr. 45 (2012) 342–350, https://doi.org/10.1107/S0021889812007662.

[37] D.I. Svergun, Restoring low resolution structure of biological macromolecules from solution scattering using simulated annealing, Biophys. J. 76 (1999) 2879–2886, https://doi.org/10.1016/S0006-3495(99)77443-6.

[38] M.B. Kozin, D.I. Svergun, Automated matching of high- and low-resolution structural models, J. Appl. Crystallogr. 34 (2001) 33–41, https://doi.org/10.1107/S0021889800014126.

[39] V. V Volkov, D.I. Svergun, Uniqueness of {\it ab initio} shape determination in small-angle scattering, J. Appl. Crystallogr. 36 (2003) 860–864, https://doi.org/10.1107/S0021889803000268.

[40] S.A. Watt, A. Wilke, T. Patschkowski, K. Niehaus, Comprehensive analysis of the extracellular proteins from *Xanthomonas campestris* pv. *campestris* B100, Proteomics 5 (2005) 153–167, https://doi.org/10.1002/pmic.200400905.

[41] A. Moutran, R.B. Quaggio, A. Balan, L.C. De Souza Ferreira, R. De Cassia Cafe Ferreira, The oligopeptide permease (Opp) of the plant pathogen *Xanthomonas axonopodis* pv. *citri*, Curr. Microbiol. 48 (2004) 354–359, https://doi.org/10.1007/s00284-003-4206-2.

[42] Y. Sugiyama, A. Nakamura, M. Matsumoto, A. Kanbe, M. Sakanaka, K. Higashi, K. Igarashi, T. Katayama, H. Suzuki, S. Kurihara, A novel putrescine exporter SapBCDF of Escherichia coli, J. Biol. Chem. 291 (2016) 26343–26351, https://doi.org/10.1074/jbc.M116.762450.

[43] S. Kurihara, S. Oda, Y. Tsuboi, G.K. Hyeon, M. Oshida, H. Kumagai, H. Suzuki, γ-glutamylputrescine synthetase in the putrescine utilization pathway of *Escherichia coli* K-12, J. Biol. Chem. 283 (2008) 19981–19990, https://doi.org/10.1074/jbc.M800133200.

[44] S. Kurihara, Y. Tsuboi, S. Oda, H.G. Kim, H. Kumagai, H. Suzuki, The putrescine importer PuuP of *Escherichia coli* K-12, J. Bacteriol. 191 (2009) 2776–2782, https://doi.org/10.1128/JB.01314-08.

[45] C.D. Lu, Y. Itoh, Y. Nakada, Y. Jiang, Functional analysis and regulation of the divergent spuABCDEFGH-spuI operons for polyamine uptake and utilization in *Pseudomonas aeruginosa* PAO1, J. Bacteriol. 184 (2002) 3765–3773, https://doi.org/10.1128/JB.184.14.3765-3773.2002.

[46] N. Killiny, Y. Nehela, Citrus Polyamines: Structure, Biosynthesis, and Physiological Functions, 2020.

[47] X.Z. Fu, Y. Huang, F. Xing, C.P. Chun, L.L. Ling, L. Cao, L.Z. Peng, Changes in free polyamines and expression of polyamine metabolic genes under drought and high-temperature in Citrus sinensis, Biol. Plant. (Prague) 60 (2016) 793–798, https://doi.org/10.1007/s10535-016-0636-0.

[48] S.R. Cockerell, A.C. Rutkovsky, J.P. Zayner, R.E. Cooper, L.R. Porter, et al., *Vibrio cholerae* NspS, a homologue of ABC-type periplasmic solute binding proteins, facilitates transduction of polyamine signals independent of their transport, Microbiol. 160 (2014) 832–843, https://doi.org/10.1099/mic.0.075903-0.